Land surface temperature assessment in relation to land-use/land-cover (A case study: Isfahan City, Central Iran)

Sayyad Asghari Saraskanrood*, Bahareh Asadi, Ehsan Ghale

Department of Physical Geography, Faculty of Social Sciences, University of Mohaghegh Ardabili, Ardabil, Iran

* Corresponding author's E-mail: s.asghari@uma.ac.ir

ABSTRACT

Most of critical issues such as increase in pollution levels, sudden climatic changes and the rise of temperature in the urban area, leading to the formation of Urban Heat Islands (UHI), have been resulted from urbanization. As population density increases, most terrestrial areas become cities, and cities grow very fast. The reason to do the current study is to compare Single-Channel, SEBAL and Split-Window methods and then choose the best method for estimating land surface temperature. The objectives are as follows: Three independent studies were conducted using a series of Landsat data: (i) to land-use/land-cover (LU/LC) classification by object-oriented method and change detection; (ii) to understand the connection between particular LU/LC class and Land Surface Temperature(LST); and (iii) LST recovery using Single-Channel, SEBAL and Split-Window, as well as comparing these methods together. The results of land-use classification and change detection indicated that urban areas have increased, while agriculture has declined. The results of validation of the three temperature recovery methods demonstrated that due to using two thermal bands simultaneously, the Split-Window method functions better and in these three algorithms, water bodies and wet soils exhibit minimum surface temperatures. Due to less vegetation, areas such as deserts, saline soils and residential area display a higher surface temperature. Vegetation has always been an obstacle for heat input and inversely related to surface heat. In addition, due to fuel pollution of machinery and factory, urban areas experience high temperatures. The only gap of this study was the utilizing 5-cm surface temperature data, which was only available at airports and was not available.

Keywords: Single-channel, SEBAL, Split-window algorithm, Object-oriented.
Article type: Research Article.

INTRODUCTION

Climate change, especially in urban areas, has received major attention due to its effects on humans, biodiversity and the urban ecosystem (Jain *et al.* 2020). Particularly, the transition from the surface of the natural earth to the impenetrable layer of the city can lead to significant climate change in the region (Weng & Lu 2008; Zhang *et al.* 2009; Liu *et al.* 2014). The unprecedented changes of landscape and human appropriation significantly dismantle the energy exchange between the earth surface and the atmosphere, leading to increase in the urban ambient temperature that deviates from the surrounding non-urbanized areas (Buyantuyev & Wu 2010; Ramezani & Ramezani 2021; Gholizadeh *et al.* 2021; Ameer Abbas 2022; Surya Suamba *et al.* 2022). The effect of urban morphology on building energy performance draws more and more attentions nowadays as building energy use accounts for over a quarter of the total energy use by cities. By a rapid urbanization of cities, the morphology of urban blocks develops from the single and low-density type to the diversified and high-density one, which has great influence on the underlying ground surface conditionings, ventilating performance and heat gain at a district scale, thus enhancing urban heat island effect and upraising building energy consumption (Zhou *et al.* 2017). Advanced models and techniques are required to describe this process, especially for typical urban-suburban areas. Particularly, the transition from natural land surface type to urban impervious layer can result in significant

regional climate change. Urban thermal environments are considered as a typical study variable by many authors (Weng & Lu 2008; Zhang *et al.* 2009; Liu *et al.* 2014). The development of thermal remote sensing provides a suitable solution for the fracture observed in the normal monitoring of urban heat islands. Such techniques can quantitatively and effectively monitor the distribution characteristics of urban heat islands as well as the periodic and dynamic changes in urban thermal environments (Pongracz *et al.* 2010). A more detailed analysis about the effects of the urban land use coverage on the distribution of urban land surface temperature (LST) as well as the scope and intensity of urban heat island, are useful for understanding the underlying mechanisms and evolution of urban heat islands (Wang *et al.* 2019). LST is an important parameter for monitoring the energy level of the surface, since the main variable determines the upward thermal radiation and it is one of the main controllers of the sensitive and latent heat flux between the surface and the atmosphere (Trigo *et al.* 2009). In recent decades, there have been proposed various algorithms for estimating the actual surface temperature using various sensors. The basis of these algorithms is based on various assumptions and approximations of radiation equations. The difference between these methods is in the number of bands used, mathematical algorithms and statistical methods for calculating atmospheric and ground emission changes to determine coefficients and computational constants. In general, atmospheric effects and emissions are two important factors in calculating surface temperature (Sekertekin *et al.* 2020). Investigations show that urban areas are warmer than the surrounding rural ones and this phenomenon, generally called urban heat island. The heat emitted from urban structures plays the most important role in urban heating, especially the heat island of the city, and it is necessary to seriously consider ways to reduce the heat island of the city. Faqe Ibrahim (2017) in a study examined using urban lands in changing land cover and their effects on land surface temperature in Dohuk City, Iraq. A Split-Window algorithm was used to achieve LST exhibiting that land use alterations and land cover affect LST. In addition to being affected by land cover and land use, LST is also very sensitive to temperature and humidity, than water. So that, the forest areas, with lower temperatures and also are man-made and urban areas, display higher temperatures. Nurwanda & Tsuyosh (2018) in a study analysed land use change and development of urban thermal islands in Bogo City, Philippines by remote sensing, which used images of Landsat TM and Landsat 8 OLI / TIRS. The results of this study showed that the highest temperature is related to urban areas, while the lowest to plant areas. In another study, Asghari Saraskanroud *et al.* (2019) investigated the relationship between different land uses and surface temperature based on spatial autocorrelation analysis (Moran) using Landsat 8 (OLI) satellite image data in Ardabil, North-western Iran exhibiting that urban areas have higher temperatures compared to water ones due to their heat absorption. In the above context, a reliable and long-term estimate of LST is very important for a large number of applications. Therefore, given the importance of the subject and the studies performed by other authors, in this study, the temperature estimate of Isfahan City is evaluated using different algorithms of measuring distance in an 18-year period and comparing the results with land use changes to determine to what extent is the surface temperature affected by land use.

MATERIALS AND METHODS

Isfahan, a tourist and industrial city in Central Iran by longitudes 51° 50′ E and 51° 78′ E and latitudes 32° 50′ N and 32° 80′ N, covers an area of approximately 550 km^2. Its topography is generally low around the Zayandeh Rud (1550 m) and high in the mountain (1650 m). The location of the study area was presented in Fig. 1. Land use and detecting changes in the maps of Isfahan was performed using object oriented algorithm obtained by Landsat 8(OLI) and Landsat 5(TM) image (Fig. 4). As a result, using the object oriented algorithm, eight land use categories were distinguished including, saline, desert, residential, water cultivation, fallow, rain-fed cultivation, water bodies and Gavkhuni Wetland in the selected region. The object-oriented classifier yields an overall accuracy of 97.25 % in 2000 and 96.19% in 2018. Also the kappa coefficient in 2000 and 2018 were 0.95 and 0.93 respectively (Table 3). Residential areas exhibited an increasing trend with an area of 33359.13 ha in 2000 and 33603.66 in 2018. Furthermore, 2207.88 ha of agricultural land has become residential areas. Moreover, most of the land turned into the residential, belonged to the desert parts with an area of 11864.73 ha. From 2000 to 2018, due to the water shortage, water cultivation declined, by 10.10357 ha turning into desolate and fallow areas. The study primarily aimed to compare the performance of the most common methods for LST retrieval from Landsat-5 TM and Landsat-8 TIRS images of Single-Channel (SC) method by Jiménez-Muñoz & Sobrino, Split-Window and Surface Energy Balance. Then, the relationships between land use/land cover (LULC) and LST in Isfahan City were examined. The LST Landsat (TM, TIRS) images in July and June (2000 and 2018) were

obtained from the US Geological Survey (USGS; https://earthexplorer.usgs.gov/). The details of the acquired Landsat image are given in Table 1.
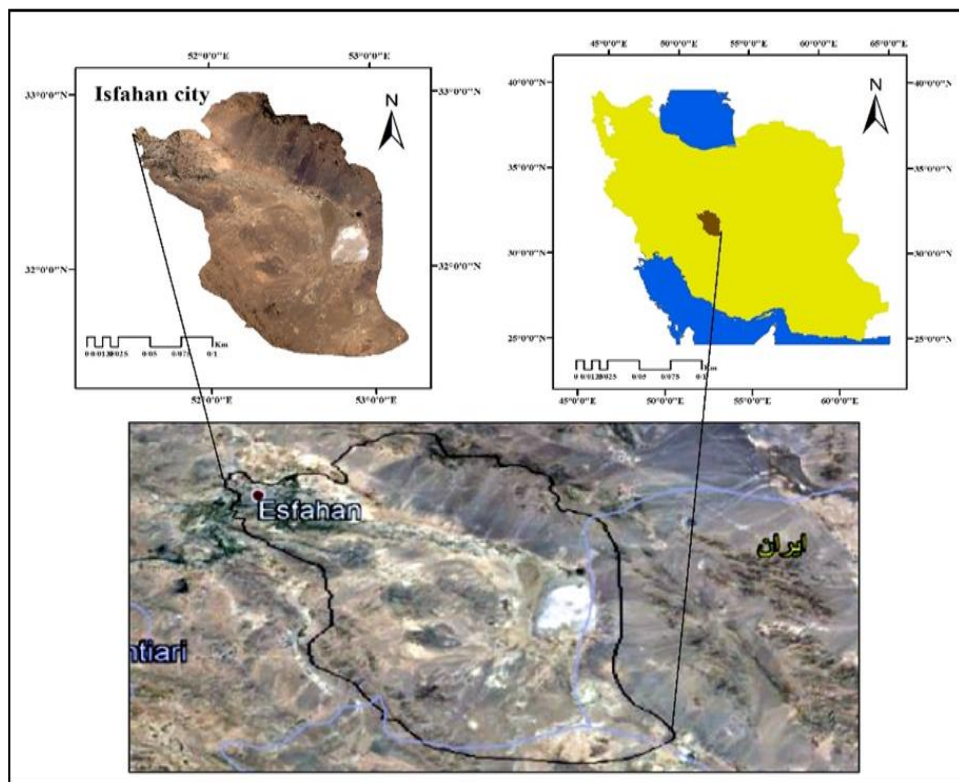

Fig. 1. Geographic location of the study area.

The obtained Landsat (level L1T) images were geometrically and topographically corrected. All the images were in Universal Transverse Mercator (UTM) projection system (zone 39 North for KMA) with WGS-84 datum. Necessary atmospheric corrections such as noise and haze correction were performed on every image before mosaicking using ENVI 5.3. For validation of the results, meteorological data obtained from the Meteorology Research Center in Isfahan Province, Iran was used, while eCognition Developer 64 software was employed for classification of lands with object oriented algorithm. In the presented study, using Landsat 8 (TIRS) and Landsat 5 (TM) image for Isfahan City, land surface temperature is calculated in three ways, i.e., Single-Channel, Split-Window and SEBAL. Then the relationship of each land use with surface temperature was investigated. The accuracy could be obtained by comparing the results of the three methods. Surface temperature was calculated using the SEBAL and Single-Channel method in 2000.Then, by SEBAL method and using the Normalized Difference Vegetation Index (NDVI) and Leaf Area Index (LAI) the surface radiation was calculated, then the land surface temperature was obtained using the formula provided. Notably, the SEBAL method uses a band 10 (Thermal -TIRS), while the single-band method uses a thermal band 6 (TM). In the case of Split-Window method, both thermal bands of Landsat 8, bands 10 and 11, were used to calculate the temperature. In this method for estimating the surface radiation, the Fraction Vegetation Cover was used and then by using the aforementioned formulas, the land surface temperature was estimated for the study area. The results indicated that, the maximum temperature of the earth is found in lands of desert and arid area, while the minimum temperature was observed in the areas of water and dense vegetation.

The Jiménez-Munoz and Sobrino's Single-Channel
Single-Channel is one of the most widely used methods for calculating the land surface temperature, which is used in many remote sensing projects. This algorithm uses the Brightness temperature images, thermal radiation and land surface emissivity. In this method, special emphasis is placed on estimating the water vapor in the atmosphere. In this study, this method was used to calculate the land surface temperature of TM. The main goal of the Single-Channel method is to obtain an algorithm to retrieve LST from one thermal band of the sensor

(Sobrino *et al.* 2004). Jime´nez-Mun˜oz & Sobrino (2003) have developed a generalized Single-Channel method in order to retrieve LST from only one thermal channel, in which the LST is given by the following equations (1-6).

$$T_S = \gamma[\varepsilon^{-1}(\psi_1 L_{sensor} + \psi_2) + \psi_3] + \delta \qquad (1)$$

With

$$\gamma = \{\frac{C_2 L_{sensor}}{T_{sensor}^2}[\frac{\lambda^4}{C_1}L_{sensor} + \lambda^{-1}]\}^{-1} \qquad (2)$$

$$\delta = -\gamma L_{sensor} + T_{sensor} \qquad (3)$$

where L_{sensor} is at-sensor radiance in Wm^{-2} sr$^{-1}\mu$m^{-1}, T_{sensor} is at-sensor brightness temperature in K, C$_1$ = 1.19104 10^8 Wμm^4 m^{-2} sr^{-1} and C$_{2=}$ 14387.7μm. The atmospheric function ψ_1, ψ_2 and ψ_3 can be obtained as a function of the total atmospheric water vapor content (w) according to the following equations particularized for TM6 data:

$$\psi_2 = -1.1836w^2 - 0.37607w - 0.52894 \qquad (4)$$

$$\psi_3 = -0.04554w^2 + 1.8719w - 0.39071 \qquad (5)$$

$$\psi_3 = -0.04554w^2 + 1.8719w - 0.39071 \qquad (6)$$

Split-Window (SW) Algorithm for LST Retrieval

The SW algorithm is based on the different atmospheric absorption behavior of two radiometric channels within the 10-12.5 μm window region. It was initially proposed to produce the real-time surface temperature patterns for seas and water bodies where the surface was commonly assumed to be a black body. Later, it was depicted that using the SW algorithm actually minimizes the small surface emittance effect on retrieved sea surface temperature (SST), and a suitable overestimation of atmospheric water vapor absorption can compensate for the surface emittance effect in a reasonable range of atmospheric total water vapor content (Ulivieri *et al.* 1994). The SW algorithm removes the atmospheric effect using the differential atmospheric absorption in two adjacent thermal infrared channels centered at 11 and 12 μm, and finally applies the linear or nonlinear combination of brightness temperatures to calculate LST (Wan & Dozier 1996). Since it does not require accurate information about the atmospheric profiles at the time of the acquisition, a variety of SW algorithms have been developed and modified to successfully retrieve LST from several sensors. Based on the new refinement of the generalized SW algorithm, a nonlinear structure of TB (as described below) was adopted to obtain LST from the TIRS of Landsat 8 (Wan 2014). The proposed SW algorithm utilizes the atmospheric window in the range of 10 μm to 12 μm wavelengths for the TIRS bands (10 and 11). The basis of the SW algorithm is the radiance attenuation for atmospheric absorption, which is proportional to the radiance difference of simultaneous measurements at two different wavelengths, each of them being subject to varying amounts of atmospheric absorption (McMillin 1975). The mathematical expression for LST can be expressed as:

$$\text{LST} = TB^{10} + C^1(TB^{10} - TB^{11}) + C^2(TB^{10} - TB^{11})^2 + C^0 + (C^3 + C^4W)(1 - \varepsilon) + (C^5 + C^6W)\Delta m \qquad (7)$$

where LST is land surface temperature in Kelvin (K), C^0 to C^6 are SW coefficient values, TB^{10} and TB^{11} are brightness temperature of bands 10 and 11 in Kelvin (K) m is mean of the LSE of the TIRS bands, W is atmospheric water vapor content and Δm is the difference in the LSE (Sobrino *et al.* 2003; Zhao *et al.* 2009; Skokovic *et al.* 2014).

SEBAL (Surface Energy Balance) Method

Surface Energy Balance Algorithm for Land (SEBAL) is considered as a physically-based analytical image processing method that evaluates the components of the energy balance and determines the LST as the residual. SEBAL is based on the computation of energy balance parameters from multi-spectral satellite data.

In order to calculate the corrected thermal radiance, the emissivity in the thermal band should first be calculated, for which, the spectral radiance (Lλ), the reflectivity values in each band (ρ$_\lambda$), and the surface albedo (ε) are required.

Spectral radiance (Lλ)
The spectral radiance is the radiance energy at the top of the atmosphere, which is detected by the satellite sensors. We calculated the spectral radiance for each band using the following equation.

$$L\lambda = \frac{L_{\max} - L_{min}}{255} . DN - L_{min} \tag{8}$$

where DN is the degree of greyness of the pixels and Ll is in ($W/m^2/sr/mm$). $L_{\max}$ and L_{min} are the calibration constants of the sensor, equal to the maximum and minimum values of the spectral radiance (in $W/m^2/sr/$ mm) detectable for each band by the sensor, in the header file of the Landsat 8 and Landsat 7 images.

Reflectivity of hemisphere (ρ_λ)
The reflectivity of a surface is the ratio of the reflected energy to the amount of energy striking the surface. The amount of reflection is calculated for each band using the following equation:

$$\rho_\lambda = \frac{\pi l_\lambda}{ESUN_\lambda .COS6.d_r} \tag{9}$$

where ρ_λ is the spectral reflectivity for each band and ESUNλ is the average for each band of solar radiation striking the top of the atmosphere in ($W/m^2/$ mm). The $ESUN_\lambda$ values for the sensor are in the Metadata file. The incident angle of the sun's radiation (θ) is computed as follow:

θ = 90-β

where β is the sun's elevation obtained from the header file of the Landsat satellite image, which is available for every scene. The sun's elevation depends on geographical location and in the current study it was equal to 68.53712984 for our study area.
The inverse of the square distance between the Earth and the sun (dr), is calculated using the Duffie & Beckman (1980) equation:

$$dr = 1 + 0.033 \cos\left(DOY\frac{2\pi}{365}\right) \tag{10}$$

where DOY is the sequential day within a calendar year which. The image date of 28 July in our study, is calculated at about 209 (Header File).

The surface radiation (ε)
Surface radiation is the ratio of the thermal energy emitted from a surface to the thermal energy emitted from a black body of the same temperature. In the SEBAL method two surface radiations are used: the first for the thermal energy emitted in a narrow thermal band (ε_{NB}) of 10.5 to 12.5 μ; and the second in a broad thermal range (ε_0) of 6 to 14 μ . The ε_{NB} figure is used to calculate the surface temperature (T_s). In our model, surface radiations are calculated using the following experimental functions:
If NDVI > 0 then the following two situations are distinguished

(a) For Leaf Area Index (LAI), LAI < 3 $\qquad$ (11)
$\varepsilon_{NB} = 0.97 + 0.0033 \times$ LAI $\qquad$ (12)
$\varepsilon_0 = 0.95 + 0.01 \times$ LAI

(b) For LAI > 3 = 0.98 $\qquad\qquad$ ε0 0.98, = ε_{NB}

For water and snow, the ε NB and ε 0 filters are used.
Water: $\qquad\qquad$ NDVI <0; α < 0:47 $\qquad$ $\varepsilon_{NB} = 0.99$; ε0 = 0.985

Snow: NDVI <0; α > 0:47   εNB = 0.99; ε0 = 0.985

In the above equations α is the (i.e. the surface's albedo).

Brightness temperature (Tbb)

Brightness temperature (TB) is the microwave radiation radiance traveling upward from the top of Earth's atmosphere. To calculate the brightness temperature, the following equation is used:

$$Tbb = \frac{K_2}{ln(\frac{K_1}{L_{10}}+1)}$$ (13)

where k_1 and k_2 are the spectral radiance for thermal band. The resulting values of k_1 and k_2 were 774.8853 and 1321.0789, while L11 is the spectral radiance of band 10.

Land surface temperature (Ts)

The LST was calculated using surface temperature (Ts) equation:

$$T_S = \frac{K_2}{Ln(\frac{\varepsilon_{NB}.K_1}{R_C}+1)}$$ (14)

where K1 and K2 values in relation to sensors (TM) are 607.76 and 1260.56, respectively and for sensor (OLI) that the band was thermal 10, the values of k_1 and k_2 are 774. 88 and 1321.07 respectively.

Land use extraction

In the presented survey, LULC has been obtained from remotely sensed data using the object-oriented (nearest neighbor) Classification techniques. Image segmentation is a preliminary step in object-oriented image classification. Then the spatial information of the segmented parcels can be derived and employed in further image analysis (Gao *et al.* 2006).
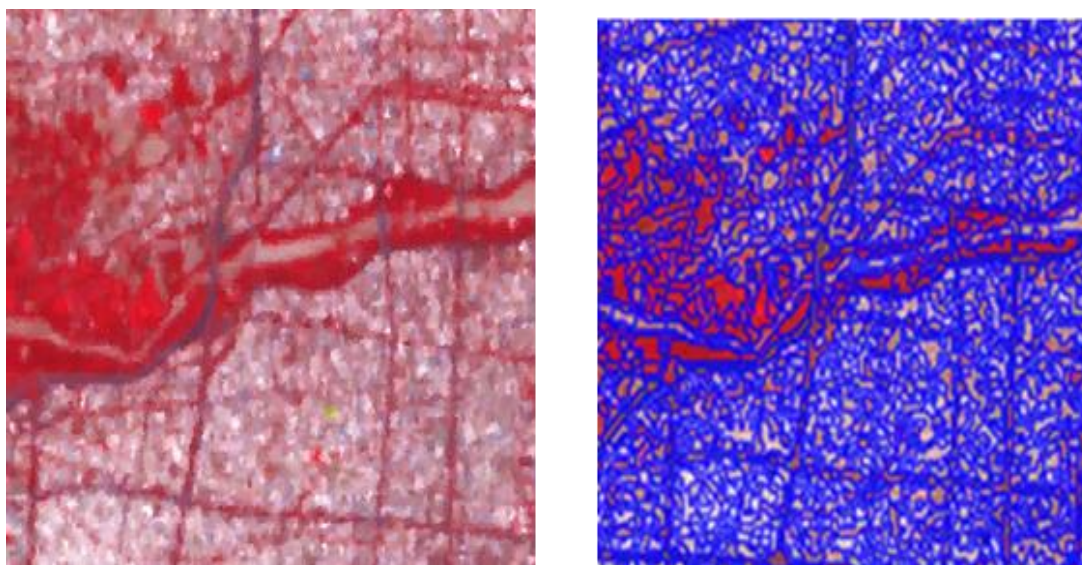

Fig. 2. Sample Image of Isfahan City (Scale: 20, Shape: 0.5, Compactness: 0.5).

Object-oriented classification was performed in eCognition, which is an object based processing software program made available in 2000 from Defines Imaging GmbH and was claimed to be user-friendly, multi-scaled, and fully functional (Blaschke & Strobl 2001). Image segmentation in eCognition is a multi-resolution, bottom up, region-merging technique starting with one-pixel objects. Image objects are extracted from the image in a number of hierarchical segmentation levels, and each subsequent level yields image objects of a larger average size by combining objects from a level below, which represents image information on different scales simultaneously. Objects are grouped into a larger object based on spectral similarity, in contrast to neighboring objects, and shape characteristics of the resulting object. These three characteristics are grouped into a single parameter called heterogeneity (Qian 2007). By a certain 'scale' parameter, three criteria define the heterogeneity

of the objects: color, smoothness, and compactness. The last two being known as shape criterion. Color criterion defines the weight the spectral values of the image layers contribute to the entire homogeneity criterion, as opposed to the weight of the shape homogeneity ((Baatz *et al.* 2004). The classifier of object-oriented image classification is nearest neighbor, which is a soft classifier, based on fuzzy logic. The nearest neighbor classifier, classifies image objects in a given feature space with given samples for the classes of concern. At First, sample objects are declared for each class, then the algorithm searches for the closest sample object in the feature space for each image object. All class assignments in eCognition are determined by assignment values in the range of 0-1. The closer an image object is located in the feature space to a sample of a class, the higher the membership degree to this class. The best classification result keeps the highest membership values (Defines Imaging GmbH 2002; Baatz *et al.* 2004). The flowchart of this study is provided in Fig. 3.
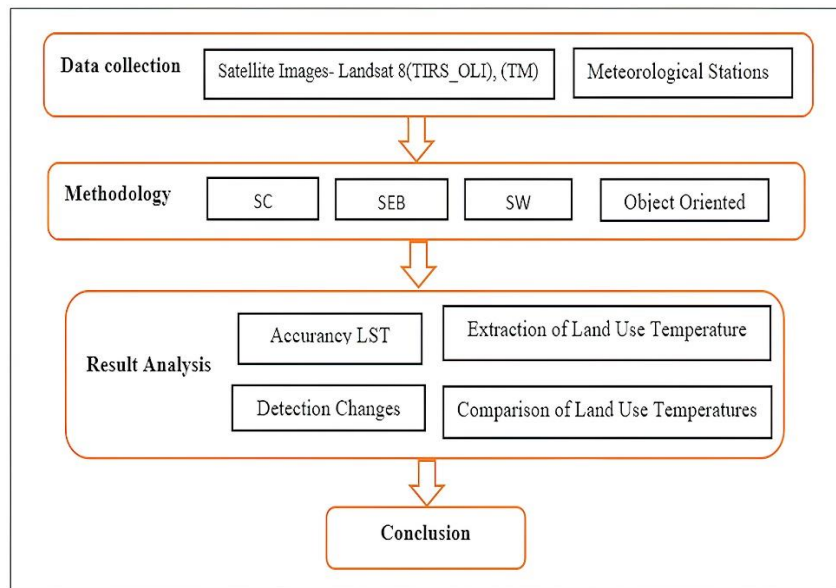

Fig. 3. Data processing flowchart.

RESULTS AND DISCUSSION

Land Surface Temperature retrieval

Land surface temperature maps of Isfahan City using Single-Channel and SEBAL methods are obtained by Landsat 5 image (TM; Fig. 4). Based on the results of the study, the maximum temperature of the earth is found in lands of desert and arid areas due to the lack of vegetation, while due to the high heat-capacity of water, the minimum temperature is observed in areas of water bodies. The desert regions in the Single-Channel method have mean temperatures of 45.31 and 43.47 in June and July respectively, whereas, in the SEBAL method, the average temperatures were 45.50 and 44.98 °C in June and July, respectively. The temperature of the other land uses are summarized in Table 1.
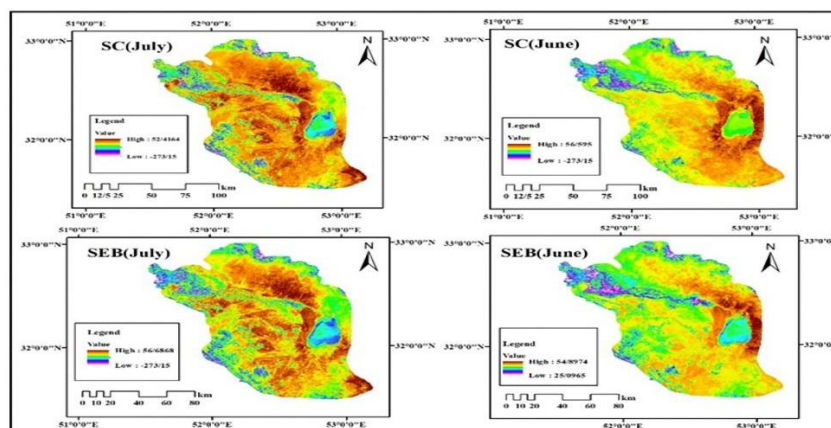

Fig. 4. LST map of Isfahan city by Single channel and SEBAL.

Table1. Comparison and statistical properties of surface temperature (in 2000).

	Land Use	Minimum Temperature	Maximum Temperature	Mean Temperatures
Temperature of each Land Use in June (2000)	Water cultivation (SC)	26.25	47.84	34.59
	Water cultivation (SEB)	13.67	49.11	13.84
	Fallow (SC)	13.22	50.28	40.45
	Fallow (SEB)	29.31	55.79	39.77
	Rain fed cultivation (SC)	27.47	74.60	38.04
	Rain fed cultivation (SEB)	25.30	53.88	31.48
	Residential (SC)	33.35	50.28	40.24
	Residential (SEB)	19.79	54.94	39.51
	Saline (SC)	16.87	46.50	41.49
	Saline (SEB)	26.60	57.68	36.32
	Desert (SC)	15.17	52.43	43.47
	Desert (SEB)	15.17	55.06	45.50
	Gavkhuni Wetland (SC)	10.83	44.82	36.63
	Gavkhuni Wetland (SEB)	27.58	49.29	39.97
	Water (SC)	19.90	43.20	17.12
	Water (SEB)	20.39	29.25	30.95

Next, the LST results are compared with the temperature measured using the 3 meteorological stations in the study area. The results exhibited that the LST estimated by the SEBAL algorithm has higher accuracy than the Single-Channel method (Fig. 5). It is concluded that the SEBAL offers better results in this study area, since this method uses band 10 of the thermal bands (10 and 11) for calculating LST, while Single-Channel method uses thermal band 6 TM for calculating LST. So, the accuracy of SEBAL algorithm is higher than the Single-Channel method. In addition, the wavelength of band 10 used in the SEBAL method is closer to the maximum wavelength of the earth's surface than the band 6 used in the TM sensor method. Fig5 depicts the comparison between surface temperature measured in the meteorological stations in the study area and those that are calculated by Single-Channel and SEBAL methods.
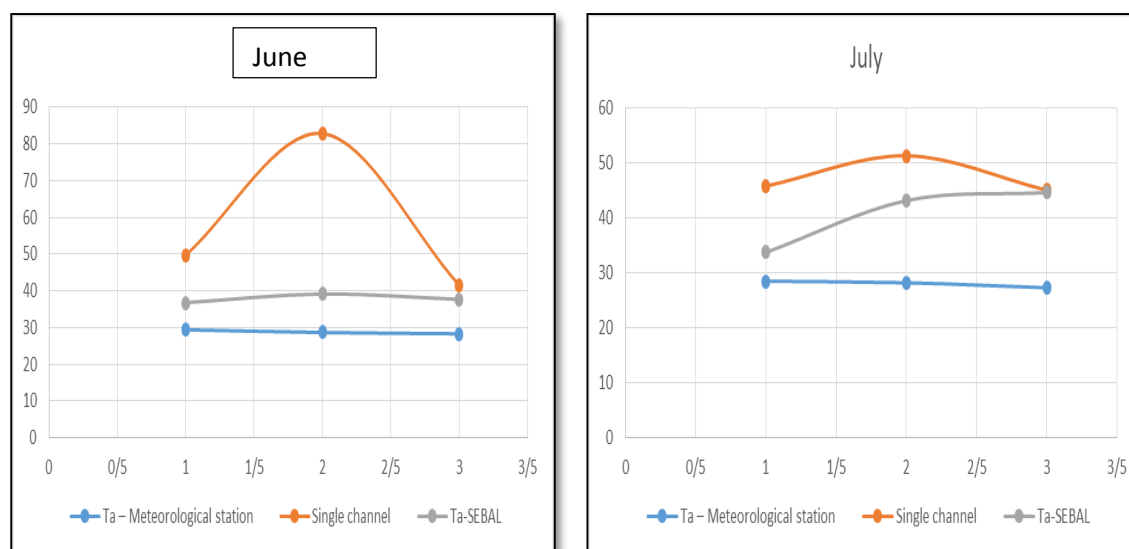
Fig. 5. Comparison among temperature of stations and those calculated by SEBAL method and Single-Channel.

Surface temperature retrieval was also performed using a Split-Window and SEBAL for the TIRS sensor in June and July (Fig. 6). In both of these methods, desert and saline regions exhibited maximum, while water bodies minimum temperatures. The desert regions in the SEBAL method displayed the mean temperatures of 44.10 and 47.11 respectively in June and July, whereas, in the Split-Window method, the average temperatures were 52.04 and 46.06 °C, respectively, in June and July. The temperature of the other land use is summarized in Table 2. It is concluded that the Spilt-Window offers better results in this study area, since this method uses two thermal bands (10 and 11) for calculating LST, while SEBAL method uses just one thermal band (10) for calculating LST, so the accuracy of Split-Window algorithm is higher than SEBAL method.
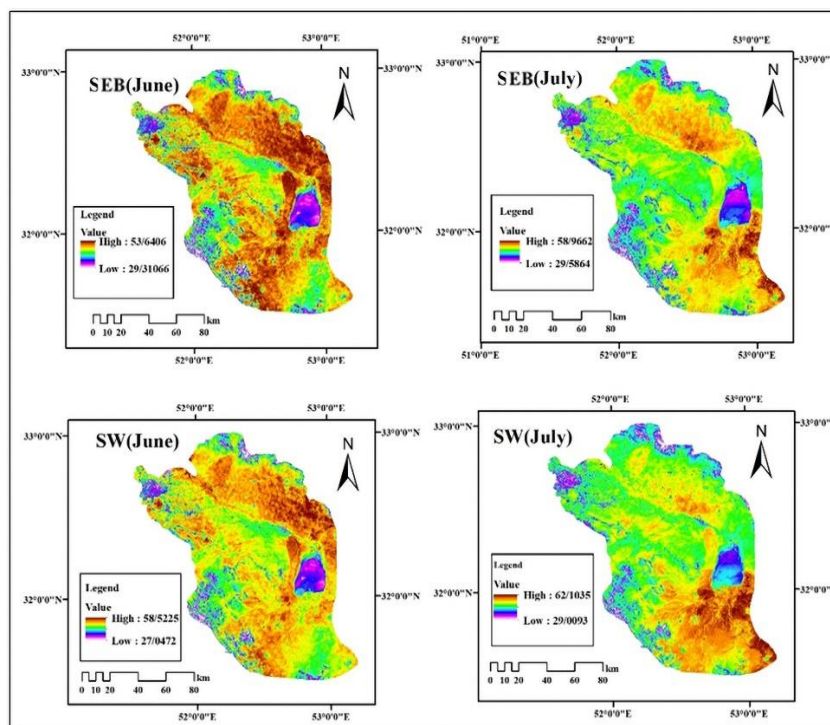
Fig. 6. LST map of Isfahan City by the Split-Window and SEBAL.

Table 2. Comparison and statistical properties of surface temperature (2018).

	Land Use	Minimum Temperature	Maximum Temperature	Mean Temperatures
Temperature of each Land Use in June (2018)	Water cultivation (SW)	32.28	50.74	40.76
	Water cultivation (SEB)	4.94	48.98	36.91
	Fallow (SW)	29.96	56.64	46.100
	Fallow (SEB)	8.9	53.64	43.18
	Rain fed cultivation (SW)	31.93	54.12	43.98
	Rain fed cultivation (SEB)	24.25	51.14	40.53
	Residential (SW)	29.68	54.54	42.24
	Residential (SEB)	7.11	51.63	39.00
	Saline (SW)	26.55	56.68	46.68
	Saline (SEB)	23.52	47.40	43.22
	Desert (SW)	31.74	49.44	46.06
	Desert (SEB)	0.56	53.52	44.10
	Gavkhuni Wetland (SW)	32.74	50.61	34.56
	Gavkhuni Wetland (SEB)	26.49	48.88	34.56
	Water (SW)	27.14	43.30	32.09
	Water (SEB)	0.44	39.32	17.36

CONCLUSION

Land surface temperature (LST) is considered as a key parameter in the physics of the earth surface through the process of energy and water exchange with the atmosphere, which plays an important role in a wide variety of scientific studies, such as ecology, hydrology, and global change studies (Kamran *et al.* 2015). Satellite images are considered as an efficient technology in calculating land surface temperature. Nowadays, using remote sensing methods, such as satellite imagery is considered as one of the efficient and important tools for displaying environmental changes and managing environmental areas. So, in the present study, Landsat 5 and 8 satellite images were employed to classify different uses during the years 2000 and 2018 in the region, and then to evaluate the accuracy of classification methods in order to found the best way to classify. The results revealed that the nearest neighbor algorithm in the object-oriented method has a kappa coefficient and that, the overall accuracy in the image classification method was higher than in the maximum probability algorithm, since the object-oriented method uses the shape coefficients, scale, compactness coefficient and vegetation index, as well as standard deviation to achieve high accuracy. The results obtained from Single-Channel and SEBAL methods exhibited that the maximum temperature of the earth is found in lands of desert and arid areas due to the lack of vegetation,

while due to the high heat-capacity of water, the minimum temperature was observed in areas of water bodies. The desert regions in the Single-Channel method exhibited the mean temperatures of 45.31 and 43.47 in June and July, respectively, whereas, in the SEBAL method, the average temperatures were 45.50 and 44.98 °C in June and July, respectively. Also, it was found that based on the results obtained from the Split-Window and SEBAL methods, desert and saline regions exhibit maximum temperatures, while water regions display minimum. The desert regions in the SEBAL method had a mean temperatures of 44.10 and 47.11 in June and July, respectively, whereas, in the Split-Window method, the average temperatures were 52.04 and 46.06 °C, in June and July, respectively. The results of this study are in line with the findings of other authors (Motlagh & Arkhi 2015; Valizadeh Kamran 2016; Asghari & Emami 2015; Feizizadeh & Helali 2009; Orac *et al.* 2004; Estileli *et al.* 2018). It is also found that the object-oriented classification is the most accurate method for extracting land use maps. After classification, the output of user maps of the object-oriented method was used to detect changes due to higher accuracy. The results showed that during the period from 2000 through 2018, residential use has increased, while agricultural use has declined due to the drying up of the river and it has become desert areas and fallow use. Land surface temperature is one of the important parameters in the study of cities, since the air temperature of the lower layers of the urban atmosphere, which is the center of energy exchange, determines the climate between buildings and affects the life and comfort of urban residents. The results of the present study showed that the surface temperature in each area is affected by the kind of utilizing the area. As it can be observed from the tables and figures, the lowest temperature is allocated to water use, while the highest to desert areas without vegetation. Also, the results of comparing three Split-Window algorithms, Single-Channel and SEBAL revealed that the Split-Window method is more accurate in calculating the land surface temperature due to using two thermal bands and the results of this method are closer to ground data.

REFERENCES

Ameer Abbas, GA 2022, Assessment of land sensitivity to desertification for Al-Mussaib project using MEDALUS approach. *Caspian Journal of Environmental Sciences*, 20: 177-196.

Blaschke, T, & Strobl, J 2001, What's wrong with pixels some recent development interfacing remote sensing and GIS. *GeoBIT/GIS*, 14: 12-17.

Buyantuyev, A & Jianguo, W 2010, Urban heat islands and landscape heterogeneity: linking spatiotemporal variations in surface temperatures to land-cover and socioeconomic patterns. *Landscape Ecology*, 25: 17-33.

Gao, Y, Mas, JF, Maathuis, BHP, Zhang, X, & Van Dijk, PM 2006, Comparison of pixel-based and object oriented image classification approaches-a case study in a coal fire area, Wuda, Inner Mongolia, China. *International Journal of Remote Sensing*, 27: 4039-4055.

Gholizadeh, M, Rezvani, SA & Zibaei, M 2021, Effects of land use change on macroinvertebrate community composition in upper reaches of the Chehel-Chai catchment, Iran. *Caspian Journal of Environmental Sciences,* 19: 523-533

Jain, S, Sannigrahi, S, Sen, S, Bhatt, S, Chakraborti, S, & Rahmat, S 2020, Urban heat island intensity and its mitigation strategies in the fast-growing urban area. *Journal of Urban Management*, 9: 54-66.

Jiménez-Muñoz, JC, & Sobrino, JA 2003, A generalized single-channel method for retrieving land surface temperature from remote sensing data, *Journal of Geophysical Research: Atmospheres*, 108(22): 19-31.

Kamran, K.V, Pirnazar, M, & Bansouleh, V.F 2015, Land surface temperature retrieval from Landsat 8 TIRS: comparison between split window algorithm and SEBAL method, In Third International Conference on Remote Sensing and Geoinformation of the Environment, pp. 9535-9550.

Liu, K, Xueling, W, & Young, M 2014, Effect of bentonite/potassium sorbate coatings on the quality of mangos in storage at ambient temperature. *Journal of Food Engineering*, 137: 16-22.

McMillin, L.M 1975, Estimation of sea surface temperatures from two infrared window measurements with different absorption. *Journal of Geophysical Research*, 80(36): 5113-5117.

Pongrácz, R, Bartholy, J, & Dezső, Z 2010, Application of remotely sensed thermal information to urban climatology of Central European cities. *Physics and Chemistry of the Earth,* 35: 95-99.

Qian, J, Zhou, Q, & Hou, Q 2007, Comparison of pixel-based and object-oriented classification methods for extracting built-up areas in arid zone, In ISPRS Workshop on Updating Geo-spatial Databases with Imagery & the 5th ISPRS workshop on DMGISs, 36: 163-171.

Ramezani, H & Ramezani, F 2021, Status and trend analysis in landscape pattern through field-based sampling

data *Caspian Journal of Environmental Sciences*, 19: 469-481.

Sekertekin, A, & Bonafoni, S 2020, Land surface temperature retrieval from Landsat 5, 7, and 8 over rural areas: assessment of different retrieval algorithms and emissivity models and toolbox implementation, *Remote Sensing*, 12(29): 1-32

Sobrino, J.A, Jimenez-Munoz, J.C, El-Kharraz, J, Gómez, M, Romaguera, M, & Soria, G, 2004, Single-channel and two-channel methods for land surface temperature retrieval from DAIS data and its application to the Barrax site, *International Journal of Remote Sensing*, 25: 215-230.

Surya Suamba, IB, Anom Wiryasa, NM, Acwin Dwijendra, NK, Agung Diasana Putra, IDG 2022, Characteristics and deviation patterns of agricultural land use in tourism area of Canggu, Bali, Indonesia. *Caspian Journal of Environmental Sciences,* 20: 423-430.

Trigo, I, Freitas, S, Bioucas-Dias, J, Barroso, C, Monteiro, I, & Viterbo, P 2009, Algorithm theoretical basis document for land surface temperature (LST)(SAF/LAND/IM/ATBD_LST/1.0), *EUMETSAT*, 14: 34-53.

Ulivieri, C, Castronuovo, M, Francioni, R, & Cardillo, A 1994, A split window algorithm for estimating land surface temperature from satellites. *Advances in Space Research*, 14: 59-65.

Wan, Z 2014, New refinements and validation of the collection-6 MODIS land-surface temperature/emissivity product. *Remote sensing of Environment*, 140: 36-45.

Wan, Z, & Dozier, J 1996, A generalized split-window algorithm for retrieving land surface temperature from space, *IEEE Transactions on Geoscience and Remote Sensing*, 34: 892-905.

Wang, W, Kai, L, Rong, T, & Shudong, W 2019, Remote sensing image-based analysis of the urban heat island effect in Shenzhen, China. *Physics and Chemistry of the Earth*, 110: 168-175.

Weng, Q, & Lu, D 2008, A sub-pixel analysis of urbanization effect on land surface temperature and its interplay with impervious surface and vegetation coverage in Indianapolis, United States. *International Journal of Applied Earth Observation and Geoinformation,* 10: 68-83.

Zhang, Y, Odeh, I.O, & Han, C 2009, Bi-temporal characterization of land surface temperature in relation to impervious surface area, NDVI and NDBI, using a sub-pixel image analysis. *International Journal of Applied Earth Observation and Geoinformation,* 11: 256-264.

Zhou, Y, Zhi, Z, Feng, Y, Yao, Y, & Xiaohong, X 2017, Urban morphology on heat island and building energy consumption, *Procedia Engineering*, 20: 2401-2406.